# Macro-Level and Genetic-Level Responses of *Bacillus subtilis* to Shear Stress

**Susmita Sahoo,[†] Rajesh K. Verma,[†] A. K. Suresh,[†,‡] K. Krishnamurthy Rao,[‡] Jayesh Bellare,[†,‡] and G. K. Suraishkumar*[,†,‡]**

Department of Chemical Engineering and School of Biosciences and Bioengineering, Indian Institute of Technology, Bombay, Powai, Mumbai 400076 India

Responses of bacterial (*Bacillus subtilis*) cells under different shear levels, from both the macro and genetic viewpoints, have been presented. The responses were studied using a novel, couette flow bioreactor (CFB), in which the entire cultivation can be performed under defined shear conditions. Oxygen supply, the normal limiting factor for entire cultivations under defined shear conditions, has been achieved by passing air through a poly(tetrafluoroethylene) (PTFE) membrane fixed on the inner cylinder of the CFB. More importantly, analyses of the oxygen transfer capabilities as well as the shear rates show that in this CFB, the effects of defined shear can be studied without interference from the effects of oxygen supply. Further, the shake flask can be used as a proper control for studying the shear effects, mainly because the shear rate in the shake flask under normal shaker operating conditions of 190 rpm has been estimated to be a negligible 0.028 $s^{-1}$ compared to a value of 445 $s^{-1}$ at the lowest rpm employed in the CFB. At the macro level the cell size decreased by almost 50% at 1482 $s^{-1}$ compared to that at 0.028 $s^{-1}$, the growth rate increased by 245%, and the maximum cell concentration increased by 190% when the shear rate was increased from 0.028 to 1482 $s^{-1}$. The specific intracellular catalase level increased by 335% and protease by 87% at 1482 $s^{-1}$ as compared to the control cultures at a shear rate 0.028 $s^{-1}$. In addition, the specific intracellular reactive oxygen species level (siROS) at the highest shear rate was 9.3-fold compared to the control conditions. At the genetic level we have established the involvement of the transcription factor, $\sigma^B$, in the bacterial responses to shear stress, which was unknown in the literature thus far; the $\sigma^B$ expression correlated inversely with the siROS. Further, through experiments with ROS quenchers, we showed that ROS regulated $\sigma^B$ expression under shear.

## Introduction

Hydrodynamic or shear stress, at sublytic levels, significantly affects the macro-level cell responses such as morphology, growth, and productivity (*1*−*5*). The macro-level responses result from altered genetic-level responses to the shear stress (*6*). Although shear is normally perceived to be deleterious, it can also be beneficial (*7*, *8*). Since shear affects cells at a fundamental level, a better understanding of its effects on cells in culture could lead to the design of appropriate bioreactors, or the operation of existing bioreactors in favorable regimes.

Studies on the effects of and cell responses to shear are available (*6*, *9*−*11*) predominantly on mammalian, plant and insect cells, and molds. However, information on shear responses of bacterial cells, which are widely used in a variety of industries, including those producing high-value products such as pharmaceuticals and other recombinant products, is not as abundant (few studies exist, e.g., *7*, *8*, *12*−*14*); the information on genetic-level responses of bacterial cells to shear is not available.

Many studies on shear effects have been reported in stirred tank bioreactors, in which it is difficult to decouple the effects of shear and oxygen transfer. For example, increase in rpm to increase shear rate would also result in an increase in the volumetric oxygen transfer coefficient. Further, it is difficult to quantify the shear levels in a stirred tank, and the average shear rate may not be representative of the actual range of shear levels to which the cells are exposed in the vessel. However, shear studies in the couette flow regime, which is achieved in the space between two concentric cylinders rotating at different angular velocities are available. Although the defined and uniform shear field in couette flow facilitates analysis, it is nontrivial to supply oxygen to aerobic cultures at adequate rates without affecting the flow field for the entire duration of growth. One is therefore constrained to device short-time experiments (e.g., *3*), or to introduce the oxygen/air in a manner that might compromise the defined shear field. In their studies on *A. niger* for example, Mitard and Riba (1988) provided oxygen by sparging air into the annular space of their couette flow bioreactor. The effect of such sparging on the flow field is uncertain.

In this work, a couette-flow bioreactor (CFB) has been designed and fabricated to cultivate cells under well-defined laminar shear conditions for the entire duration of growth. The CFB was designed to ensure operation in the couette-flow regime (by using a thin annulus) as well as to ensure oxygen supply without compromising the laminar flow profiles, so that long-term cultivations of

* To whom correspondence should be addressed. Phone: +91 (22) 2576 7208. Fax: +91 (22) 2572 6895/3480. E-mail: gksuresh@che.iitb.ac.in.

[†] Department of Chemical Engineering.

[‡] School of Biosciences and Bioengineering.

10.1021/bp034191w CCC: $25.00 
Published on Web 00/00/0000 

B

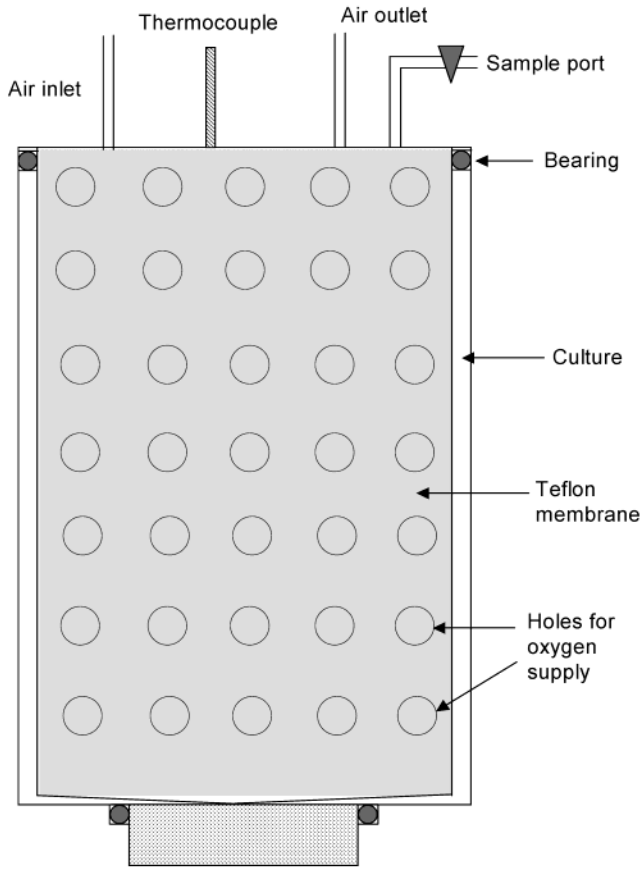


**Figure 1.** A schematic diagram of the couette flow bioreactor (CFB) with a provision to supply oxygen without disturbing the flow pattern.

an aerobically growing organism can be carried out in a defined shear environment. The problem of oxygen supply with minimum disturbance to the flow field was addressed by having oxygen inside the hollow inner cylinder and transferring it to the annular space containing the culture across an oxygen-permeable membrane.

Using the CFB, the responses of *Bacillus subtilis* cells when grown under well-defined laminar shear conditions were studied. *Bacillus subtilis* was chosen as the model system, because it is one of the preferred hosts in bioindustry and has been well studied. Also, it is nonpathogenic, relatively simple to cultivate, and secretes a variety of proteins and metabolites. In the sections to follow, analyses of the shear rate and mass transfer aspects in the CFB and their comparison with shake flask show that the shake flask can be used as the "control" for shear studies. The effect of shear on the macro-level aspects such as morphology, growth, and enzyme productivity are presented. Also, since reactive oxygen species (ROS) are suspected to be the mediators of many stresses (*15*), the effect of shear on specific intracellular reactive oxygen species level (siROS) was studied. Further, the involvement of the transcription factor, $\sigma^B$, in the shear response of cells was explored. Also, the relationship between (siROS) and expression of $\sigma^B$ was investigated.

## Materials and Methods

The cultivations of *B. subtilis* were carried out in two types of devices in the present work. The first was a standard shake flask of 500 mL capacity, while the other was the CFB designed and fabricated as a part of this work.

**Couette Flow Bioreactor (CFB).** Figure 1 shows a schematic of the CFB, fabricated at Vaspan Industries, Mumbai, India. The bioreactor has the inner cylinder stationary and the outer cylinder rotating, a configuration that stabilizes the flow and allows operation at higher Reynolds numbers (*16*) as compared to the alternative configuration of inner cylinder rotating and the outer stationary. The reactor has been designed to be able to accommodate a culture volume of 250 $cm^3$ in the annular space. Care has been taken to see that the thickness of the annular region is small compared to the outer radius, the ratio of radii of the inner to the outer cylinder being about 0.93. Similarly, the height occupied by the culture volume in the annulus is sufficiently large as compared to the thickness of the annular region (the ratio being 76.05) so that end effects are negligible. A uniform shear field can therefore be assumed to exist in the annular space when the device is operated.

The inner cylinder is hollow, and a regular square array of 10 mm diameter holes is made in the curved surface to provide the mass transfer area for oxygen. A poly(tetrafluoroethylene) (PTFE) membrane is stuck over this surface, with care taken to smooth out any wrinkles. A port is provided to admit air into the hollow space inside the inner cylinder, and oxygen from this space diffuses across the membrane and is transferred into the culture by a process of convective diffusion.

Ports are provided for sample withdrawal and for a thermocouple, with care taken care not to interfere with the flow pattern. The entire assembly is housed in a Plexiglas enclosure so that the desired temperature can be maintained by controlling the temperature of air in the enclosure. The whole reactor, with the membrane in place, is autoclaved prior to cultivation, and the culture is transferred under the sterile conditions provided by a laminar hood.

***Cell Strains, Media, and Cell Treatment.*** *Bacillus subtilis* 168 *(trpC*2) (BGSC, Ohio State University, Columbus, OH) cultures were stored at −20 °C in LB liquid media (Hi-media) containing 15% glycerol. The *sigB* null-mutant of *B. subtilis (sigB::ΔHindIII-EcoRV::cat trpC*2, BSA272, (*17*)) was kindly provided by Prof. W. Haldenwang, Department of Microbiology, University of Texas, San Antonio, TX. The *sigB-lacZ* strain of *Bacillus subtilis (amyE::sigB-lacZ trpC*2, PB286, (*18*)) was a kind gift from Prof. C. W. Price, Food Science Department, University of California, Davis, CA. PB286 carries a transcriptional fusion of $\sigma^B$ to the *E. coli lac Z* gene. This fusion allows $\beta$-galactosidase activity to be monitored as a measure of $\sigma^B$ expression.

The cells were grown in Luria-Bertani (LB) medium (Hi-media). The preinoculum was prepared by growing cells in liquid media at 37 °C to exponential growth phase (12 h). They were diluted 1:10 (v/v) into the fresh media and inoculated either to the CFB or to the shake flasks. The initial cell concentration was maintained at 0.5 ± 0.03 g $L^{-1}$ by adjusting the preinoculum concentration. Special care was taken for transferring the preinoculum to the autoclaved CFB, inside a laminar flow hood. The cells were grown in different shear environments (in the CFB at various rpm or, in the shake flasks, at 190 rpm) at 37 °C for 30 h. All experiments were repeated at least twice for reproducibility. The maximum variation in corresponding data points was 9%.

The antioxidant *N*-acetyl cysteine (NAC), as well as diphenylene iodoniumchloride (DPI), an inhibitor of superoxide generation, were used as treatment agents in certain studies. The concentrations of NAC and DPI used were 5 mM and 0.6 $\mu$M, respectively. The concentrations of NAC and DPI used were determined through toxicity studies; cells were exposed to different initial

**Table 1. Estimated Volumetric Oxygen Transfer Coefficients ($k_L$a) in CFB without and with PTFE Membrane on Inner Cylinder, Calculated Value of $k_L$a in Shake Flask, Shear Rates at Various rpm, and Specific Growth Rates for Different Cultivations**

| rpm | estimated $k_L$a (without membrane) ($h^{-1}$) | measured/estimated $k_L$a (with membrane in CFB) ($h^{-1}$) | shear rate ($s^{-1}$) | specific growth rate[a] ($h^{-1}$) |
|---|---|---|---|---|
| (CFB) 300 | 256 | 4.54 | 445 | 0.26 |
| (CFB) 500 | 407 | 4.56 | 741 | 0.33 |
| (CFB) 750 | 554 | 4.58 | 1111 | 0.40 |
| (CFB) 1000 | 738 | 4.59 | 1482 | 0.76 |
| (shake flask) 190 | na | 2.89 | 0.028 | 0.22 |

[a] Each specific growth rate value was obtained from the average values of cell concentrations from two/three different experiments at each shear rate.

concentrations of the two treatment agents, and the concentration that least affected the viability was chosen for treatment. NAC was added to the medium at the start of the cultivation, and cells were exposed to DPI (prepared fresh) for 5 min, separated from the treatment medium, resuspended in cell-free medium of similar nature, and grown.

**Analyses.** Samples were taken from the shake flask and the CFB at regular intervals. Each sample of approximately 5 mL was collected, and cells were separated from the supernatant (centrifugation at 12,000 × *g* for 15 min). They were stored in a deep freezer (−20 °C) until further analysis was done. For measuring intracellular ROS levels, the sample was processed immediately. Cell concentration was measured using a spectrophotometer (Shimadzu, Japan) through cell scatter measurements at 600 nm and using a calibration graph. Standard methods were followed for measuring extracellular enzyme concentrations immediately after the completion of the cultivation: the azocasein degradation method for protease (*19*), the hydrogen peroxide decomposition rate method for catalase (*20*), and the starch hydrolysis method for amylase (*21*). The standard curve was prepared using enzymes from Sigma. A standard assay procedure for $\beta$-galactosidase (*22*) was followed, and specific activity was expressed in Miller Units (MU), which was calculated as

$$\mathrm{MU} = \frac{A_{420} \times 1000}{A_{600} \times \text{reaction time in min}}$$

**Spin Labeling and Electron Spin Resonance (ESR) Spectroscopy.** One milliliter of the fresh sample was centrifuged (12,000 × g, 10 min, −4 °C) and washed thrice with saline to remove traces of media with extracellular secretions. The cells were suspended with an equal amount of 100 mM ice-cold Tris buffer (pH 8.0, saturated with $N_2$). Lysozyme 2.5 mg $mL^{-1}$, sucrose 100 mM, EDTA 132 $\mu$M, and $MgCl_2$ 2.5 mM were added, and the mixture was incubated at 37 °C for 15 min. The solution was centrifuged at 12,000 × *g*, 4 °C for 10 min. The resulting protoplasts in the pellets were washed once with the above mixture without lysozyme. To the protoplasts was added 80 mM dimethyl-1-pyrroline-*N*-oxide (DMPO, Sigma) (spin trap). Subsequently, the volume was made up to 1 mL using distilled water and mixed thoroughly to break open the protoplasts through osmotic shock. The derivative ESR spectrum was obtained immediately after, using a Varian E-112 EPR spectrometer. The final two steps were done under red light. The area under the absorption curve was obtained by double integration of the derivative ESR spectrum using a computer program, and a standard curve was used to obtain the actual ROS concentrations; the free radical concentration is proportional to the area under the absorption curve (*23*). The specific intracellular ROS level was obtained by normalizing the intracellular ROS concentrations with the corresponding viable cell number concentrations. The viable cell number concentration was determined by the plating method, and the plates were inoculated immediately after sample collection. The ROS type was identified by comparison with standard spectra in the literature (*24*).

**Sample Preparation for Scanning Electron Microscopy (SEM).** The SEM technique was used to examine the cell shape and size at high resolution. Fresh samples of cells taken from the CFB or shake flasks were used for analysis using a Quanta 200, FEI-Philips environmental scanning electron microscope (ESEM). For analysis using ESEM, a carbon-coated copper grid was dipped in the sample for 1 min and then dipped in 0.5% phospho-tungstic acid for 1 min for negative staining of the cells. They were dried with the help of Whatman No. 1 filter paper. The grids were stuck to a stub and placed on the specimen holder under vacuum. The cells were viewed under low vacuum mode at room temperature under different magnifications and acceleration voltages.

## Results and Discussion

**Oxygen Transfer Coefficient in CFB.** Although the CFB has provision for supplying oxygen without actual sparging and thereby not interfering with the flow field, it is important to make sure that the transfer rates provided for are adequate. An estimate of the mass transfer rate was obtained by measuring the volumetric mass transfer coefficient $k_L$a by a physical method as follows: the inner cylinder, with air passing in and out to maintain a constant oxygen partial pressure, was held in a vessel containing water depleted of oxygen by prior sparging of nitrogen. Oxygen tension in the water was measured as a function of time until saturation was reached. Oxygen transfer to the water in the vessel through other routes such as that across the air−water interface on the top of the vessel was avoided by using aluminum foil to cover the surface. A semilog plot of fractional saturation vs time yielded a value of 0.17 $h^{-1}$ for $k_L$a, under quiescent conditions.

The values of the volumetric oxygen transfer coefficient, $k_L$a, in the CFB under convective conditions were estimated as follows. From a plot of $j_D'$ vs *Re* for mass transfer in a rotating cylinder system (*25*) the $k_L$a values were estimated using the appropriate values for angular velocities, Schmidt numbers, and transfer areas per unit volume. The $k_L$a values, given in Table 1, show that, as expected, under convective conditions they were 3 orders of magnitude higher than those under the quiescent conditions. However, in the system employed here, the gas and the liquid phase are separated by the PTFE membrane, and it is important to account for the transport resistance due to the membrane. This can be accomplished by writing a quasi steady-state equation for the oxygen mass transfer flux $N_{O_2}$, considering the

transport processes in series:

$$N_{O_2} = \left(\frac{D}{\delta}\right)(H_1 p_{O_2} - c_\delta) = k_L(H_2 c_\delta - c_b) \quad (1)$$

where $p_{O_2}$ is the partial pressure of oxygen inside the inner cylinder, $D$ is the diffusivity of oxygen through the membrane, $\delta$ is the membrane thickness, $c_\delta$ ia the concentration of oxygen in the membrane phase at the membrane−liquid interface, and $c_b$ is the concentration of oxygen in the liquid bulk. $H_1$ is the Henry's law coefficient for oxygen for the gas−membrane system, and $H_2$ is the partition coefficient for oxygen between the membrane and the liquid. A solution-diffusion process for the transport across the membrane has been assumed, and transport resistance on the gas side has been neglected. Knowing one of $H_1$ and $H_2$ and the Henry's law coefficient $H$ for oxygen for the air−water system, the other can be calculated, as the equilibrium between air and water should not depend on whether a membrane separates the phases:

$$H = H_1 H_2 \quad (2)$$

Calculating $c_\delta$ from eq 1 and substituting in one of the right-hand sides of the same equation enable the mass transfer flux to be written in terms of an overall liquid side driving force:

$$N_{O_2} = k_{L,eff}(H p_{O_2} - c_b) \quad (3)$$

where

$$k_{L,eff} = k_L \frac{\frac{D}{\delta}}{\frac{D}{\delta} + k_L H_2} \quad (4)$$

$k_{L,eff}$ is the effective overall mass transfer coefficient that accounts for the resistances due to the membrane as well as the liquid film. Clearly, the importance of the membrane resistance depends on the thickness of the membrane for a given material. For a given membrane, the importance of its resistance, vis-à-vis the liquid side resistance, depends on the value of the latter; the membrane resistance increases in importance as the liquid side resistance decreases. For the PTFE membrane used, we have the following data at 25 °C (the diffusivity and solubility of oxygen in PTFE have been taken from http://www.sablesys.com/oxelect.html accessed on September 10, 2002): thickness ($\delta$) = 100 $\mu$m; $D = 2.54 \times 10^{-11}$ m$^2$ s$^{-1}$; $H_1 = 0.106 \times 10^{-7}$ mol (m$^3$ kPa)$^{-1}$; and $H = 1.19 \times 10^{-8}$ mol (m$^3$ kPa)$^{-1}$ (*26*). Substitution of these values gives

$$k_{L,eff} = k_L \frac{2.54 \times 10^{-7}}{2.54 \times 10^{-7} + 1.12 k_L} \quad (5)$$

Values of the effective overall volumetric mass transfer coefficient $k_{L,eff}a$ calculated from the above equation, using the estimated $k_L$ values for different rpm's in the CFB are shown in Table 1, and it is clear that the membrane resistance dominates. As a consequence, effective transfer rates are nearly constant across all of the rotation speeds used. Significantly, in the range of rpm employed, the $k_{L,eff}a$ value is between 4.54 and 4.59 h$^{-1}$, which is of the same order of magnitude as that measured in the shake flask at 190 rpm (2.89 h$^{-1}$). Thus CFB is an ideal device to study the effect of shear alone, which is not possible in stirred tanks; in stirred tanks the combined effects of shear and oxygen transfer cannot be easily decoupled when air is used as the oxygen source.

**Shake Flask Cultivations Used as Control Cultivations for Shear Studies.** Two types of devices have been used in the present cultivations, the couette flow bioreactor (at several speeds of rotation to vary the shear rate) and the shake flask. For a meaningful comparison of the results in the two devices, we need methods of calculating the shear rates in the two devices. The shear rates in the CFB can be exactly calculated from the velocity field (*27*, *28*):

$$v_\theta(r) = R\Omega \frac{r/(kR) - kR/r}{(1/k) - k} \quad (6)$$

where $k$ is the ratio of the inner radius to the outer radius $R$, and $\Omega$ is the angular velocity of the outer cylinder. Differentiating, we get the shear rate at any radial position $r$ as

$$\dot{\gamma}(r) = 2\Omega \frac{\left(\frac{kR}{r}\right)^2}{k^2 - 1} \quad (7)$$

For thin annuli ($k \rightarrow 1$), these equations predict a nearly linear profile of $v_\theta$, and hence, a nearly constant shear rate at every $r$.

For the considerably more complex and turbulent hydrodynamics prevailing in the shake flask, the shear rate can only be estimated. The energy dissipation rate in shake flasks is reasonably uniform (especially in comparison with mechanically stirred bioreactors), so that an average shear rate can be used for purposes of comparison (*28*). Extending the same argument further, such an average shear rate can be calculated for the shake flask in the following manner.

The shear stress on a particle at any location in a turbulent flow field is determined primarily by the velocity of turbulent fluctuations. The theory of isotropic turbulence visualizes eddies of a spectrum of sizes in a turbulent flow field, the energy content of the eddies decreasing with their size. In such a scenario, the stress that a particle feels in the flow field depends on the particle size relative to an appropriate length scale of turbulent eddies. Kolmogorov's microscale of turbulence $\eta_l$ is normally used as a measure of the latter and is related to the rate of energy dissipation $\epsilon$ as follows:

$$\eta_l = \left(\frac{V^3}{\epsilon}\right)^{1/4} \quad (8)$$

For the shake flask, since the rates of energy dissipation do not vary greatly across the cross section, we can associate a Kolmogorov length scale with the *average* rate of energy dissipation, calculated as the power input per unit mass. The power input for shake flasks can be calculated from (*28*):

$$\frac{P}{\rho n^3 d_s^5} = \frac{1.94}{Re^{0.2}} \frac{V_L^{1/3}}{d_s} \quad (9)$$

where the Reynolds number $Re$ is defined as

$$Re = \frac{n d_s^2}{\nu} \quad (10)$$

For the conditions relevant to our experiments, these equations give a value of $4.32 \times 10^{-5}$ m for $\eta_l$. Electron micrographs (discussed later) show the *Bacilli* grown in shake flasks to be about 1 $\mu$m in diameter and 3−4 $\mu$m in length. Since the particle dimension is almost an order of magnitude smaller than $\eta_l$, we may expect the effect of shear to be negligible in the shake flask. For such small ratios of particle diameter to the Kolmogorov scale, the determining eddies are in the dissipation range, for which the shear stress $\tau_t$ is given by the equation (*28*)

$$\frac{\tau_t}{\rho\sqrt{\upsilon\epsilon}} = 0.0676\left(\frac{d_p}{\eta_l}\right)^2 \tag{11}$$

Choosing a spherical diameter $d_p$ of 2 $\mu$m for the *Bacillus* for an estimate, we get the shear stress to be $2.8 \times 10^{-5}$ N m$^{-2}$. For water-like viscosity, this would correspond to a shear rate of about 0.028 s$^{-1}$. This value is very small, particularly when compared with the values of shear rate that can be calculated for the CFB, confirming the expectation that the *Bacilli* experience negligible shear in the shake flask. These calculations, together with those in the previous section, which show the oxygen transfer rates in the two devices to be similar in order of magnitude, therefore suggest that experiments in the shake flask can be regarded as control experiments in delineating the effects of shear on fermentation behavior.

**Cell Size.** The cell size under shear was studied using scanning electron microscopy. The average cell size obtained at 0.028 s$^{-1}$ was about 3.05 $\mu$m and reduced to about half that size when grown at 1482 s$^{-1}$ in the CFB (Figure 2). This was in contrast to our initial expectation of longer cells at higher shear rates, as observed with bacterial cells exposed to short duration of laminar shear (*7*). In any case, those authors suspected that the cell elongation was due to the added viscosity modifier. Probably, the size reduction observed in this study is due to cell adaptation mechanisms when exposed to a higher shear rate. For example, it may be an advantage in terms of stress handling for the cells to present a smaller surface to the flow around them when the levels of shear stress are high. In addition, asymmetrical cell division was noticed at shear rate 1482 s$^{-1}$; some dividing cells appeared pinched off at one end. Similar asymmetrical cell divisions were observed by Edwards et al. (1989) in *E. coli* cells at high shear levels (10.9 and 14.5 N m$^{-2}$).

**Growth and Enzyme Production.** The time profiles of cell concentration obtained at different shear rates are presented in Figure 3; the average shear rates and the corresponding rpm are presented in Table 1. Interestingly, the maximum cell concentration obtained increased with the shear rate. The maximum cell concentration obtained at the highest average shear rate studied, 1482 s$^{-1}$ (1000 rpm), was 7.8 g L$^{-1}$, which was 195% of that obtained at 445 s$^{-1}$ (300 rpm) and 289% of that obtained at 0.028 s$^{-1}$ (shake flask control at 190 rpm). The exponential specific growth rates, presented in Table 1, show that it also increased significantly with shear rate; the exponential specific growth rate at 1482 s$^{-1}$ was 292% of that obtained at 445 s$^{-1}$ and 345% of that obtained at 0.028 s$^{-1}$. Also, the cells grown at higher shear rates showed a shorter lag period as compared to the cells grown at 0.028 s$^{-1}$. The above observations that the exponential specific growth rate and maximum cell concentration increase, whereas the lag times decrease with increase in shear rate, can be utilized to reduce the cultivation time significantly in industrial bioreactors, which would improve the process economics; however, the economical achievement of higher shear rates could be a challenge.

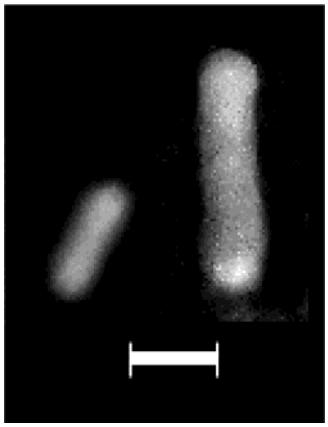

**Figure 2.** Scanning electron micrographs of cells grown in a shake flask at a shear rate of 0.078 s$^{-1}$ (right) and in CFB at a shear rate of 1482 s$^{-1}$ (left). ESEM, 8000×, 20 kV, 0.98 Torr; bar = 1 $\mu$m.

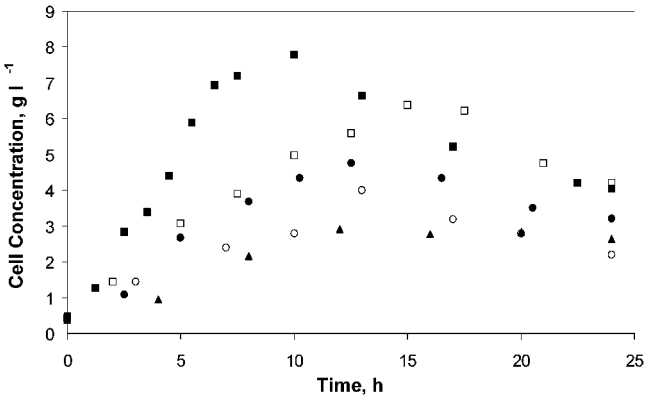


**Figure 3.** Growth profiles under various shear rates: (■) 1482, (□) 1111, (●) 741, (○) 445, (▲) 0.028 s$^{-1}$.

The maximum specific levels of extracellular enzymes, i.e., catalase, protease, and amylase, obtained at various shear rates are presented in Figure 4. From the figure, it can be seen that the specific levels of catalase increased with shear rate: the maximum specific level at 1482s$^{-1}$ was 3035 U (g-cell)$^{-1}$, which was 199% of that obtained at 445 s$^{-1}$ and 765% of that obtained at 0.028 s$^{-1}$. The extracellular protease level also increased with shear rate: the maximum specific level at 1482 s$^{-1}$, 0.73 U (g-cell) L$^{-1}$, was 252% of that obtained at 445 s$^{-1}$ and 187% of that obtained at 0.028 s$^{-1}$. The reason for the initial decrease in specific protease level with shear rate is unclear. However, the extracellular specific levels of amylase did not vary significantly with shear rate in the range studied.

**Correlation between Shear and siROS.** Reactive oxygen species are known to mediate cellular processes under many stress conditions (*15*). Also, ROS are suspected to be involved in mediating shear stress responses of animal cells (*29*, *30*). Therefore, we suspected that ROS are involved in shear stress responses of bacteria also, and the specific intracellular ROS levels were determined when the wild-type cells were grown at various shear rates. The ROS type was found out to be superoxide and superoxide-derived radicals. The 10-h siROS presented in Figure 5 clearly show that the siROS increased with shear rate; it was 3.7 mmol (g-cell) L$^{-1}$ at 1482 s$^{-1}$, which was 9.3-fold of that at 0.028 s$^{-1}$ and 4.6-fold of that at

F

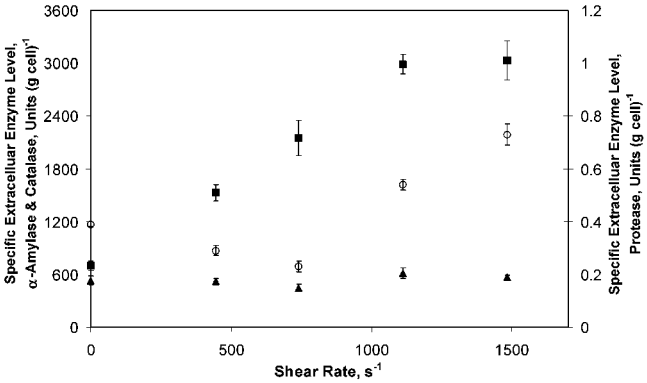


**Figure 4.** Maximum specific levels of (■) extracellular catalase, (○) protease, and (▲) α-amylase at different shear rates. The specific enzyme levels were determined by normalizing the enzyme activity with the cell concentration, at the corresponding time.

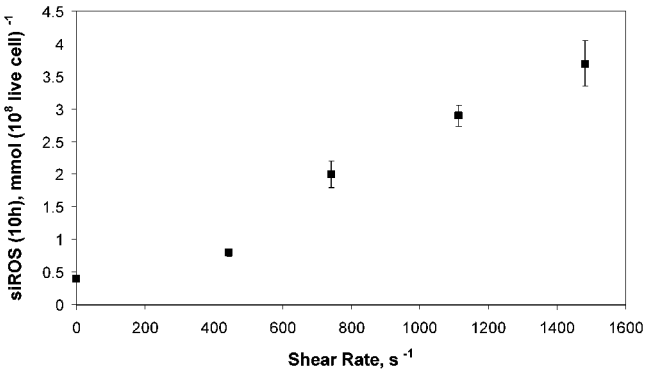


**Figure 5.** Specific intracellular reactive oxygen species levels (siROS) obtained at 10 h (maximum siROS) when cultivated at various shear rates.

445 $s^{-1}$. The siROS at other times also showed the same trend (data not shown). Therefore, it is reasonable to suggest that ROS are involved in mediating shear stress responses in *B. subtilis*.

**Genetic Basis for Shear Response; Involvement of $\sigma^B$.** To understand the different responses of the cells under shear stress, the general stress transcription factor, $\sigma^B$ was chosen for the study. $\sigma^B$-controlled genes are known to play important roles in protection against the deleterious effects of various stresses such as oxidative, heat shock, acid, ethanol, and salt stresses and nutrient depletion (*31*), although the relationship between shear stress and $\sigma^B$ is unknown thus far. Hence, we were interested in determining if $\sigma^B$ also played a role in responses to shear stress. In addition, *katE*, which is one of the genes responsible for catalase production in the stationary phase, is controlled by $\sigma^B$ at the transcription level (*32*). Therefore, we expected a reduction in the stationary-phase catalase level when $\sigma^B$ was inactive.

To investigate the above possibilities, a strain that lacks $\sigma^B$ (*sigB* null-mutant, *sigB::cat trpC2*) was compared with the wild-type strain, which produces $\sigma^B$ (*trpC2*), at the highest shear rate, 1482 $s^{-1}$. From the results presented in Table 2, it can be seen that the specific extracellular catalase level obtained with *sigB* null-mutant, *sigB::cat*, was 60% lower than that obtained with the wild-type strain. In addition, the maximum cell concentration obtained with *sigB::cat* was 25% lower than that obtained with the wild-type, indicating that the *sigB* null-mutant was more shear-sensitive compared to the wild-type strain. Under low shear conditions (0.028 $s^{-1}$), the catalase productivity and growth of the *sigB* null-mutant was comparable to those of the wild-type cell. Therefore, it is clear that $\sigma^B$ is involved in responses to shear stress and possibly protects the cells under high shear.

**Table 2. Comparison of Maximum Specific Enzyme Levels, Maximum Cell Concentrations, and Specific Growth Rates Obtained in Cultivations at 1482 $s^{-1}$ of *sigb*-null Mutant and Wild-Type Cells**

| parameter | wild-type | *sigB*-null mutant |
|---|---|---|
| maximum specific catalase level, Units (g cell)$^{-1}$ | 3035 ± 202 | 1229 ± 59 |
| maximum specific amylase level, Units (g cell)$^{-1}$ | 570 ± 22 | 368 ± 24 |
| maximum specific protease level, Units (g cell)$^{-1}$ | 0.73 ± 0.04 | 1.25 ± 0.08 |
| maximum cell concentration, g $L^{-1}$ | 7.8 ± 0.4 | 5.9 ± 0.5 |
| specific growth rate, $h^{-1}$ | 0.76 | 0.74 |
| max siROS, mmol ($10^8$ live cells)$^{-1}$ | 3.7 ± 0.4 | 11.3 ± 0.6 |

Interestingly, at 1482 $s^{-1}$ the specific extracellular amylase level with the *sigB* null-mutant was 35% lower than that with the wild-type; the growth rates of both were comparable, and the specific extracellular protease level with the *sigB* null-mutant was 71% higher than with the wild-type; the reasons for these observations are unclear.

To further investigate the relationship between shear and $\sigma^B$, we measured the transcriptional levels of $\sigma^B$ in the strain *sigB::lacZ trpC2*. The data given in Table 3 shows that the expression of $\sigma^B$ decreased with increasing shear rates. For example, the maximum transcription level of $\sigma^B$ at 445 $s^{-1}$ was 42% lower, and at 1482 $s^{-1}$ it was almost 40-fold (4000%) lower, compared to 275 MU at 0.028 $s^{-1}$. The maximum expression of $\sigma^B$ was obtained in the late-exponential/stationary phase (data not shown); the zero time values were not considered because they represent the inoculum conditions. The finding that $\sigma^B$ protects the cells even when maintained low at high shear stress can be explained on the basis of the intracellular pool of $\sigma^B$ that was carried from the inoculum; the pool may remain active and provide the protection. The pool diminishes afterward, because new $\sigma^B$ molecules are not produced under high shear. In the case of the mutant, the pool is nonexistent even in the inoculum, and therefore these cells are more sensitive to the shear stress. However, the reasons for this decreased expression of $\sigma^B$ in a highly stressed cell, where it is shown to protect the cell, is still unclear. One of the reasons could be the unusually high level of intracellular ROS (superoxide and superoxide-derived radicals) under shear stress.

**Relationship between ROS and $\sigma^B$ under Shear Stress.** To investigate the possible relationship between the stress mediator, ROS, and $\sigma^B$ expression under shear stress, we measured the siROS and the $\sigma^B$ expression at very low (0.028 $s^{-1}$), moderate (445 $s^{-1}$), and high (1482 $s^{-1}$) shear levels. The composite data in Figure 6 shows that $\sigma^B$ transcription level decreased with increase in siROS. It decreased steeply from a value of around 260 MU at 0.4 mmol (g-cell) $L^{-1}$ to about 15 MU at 1 mmol (g-cell) $L^{-1}$. It reached a basal value of about 6 MU at 2 mmol (g-cell) $L^{-1}$ siROS.

To further support the relationship between ROS and $\sigma^B$ expression under shear, we studied the transcription level of $\sigma^B$ when siROS was reduced at the highest shear rate employed, 1482 $s^{-1}$. The antioxidant, *N*-acetyl cysteine (NAC), was used to reduce siROS. In the cultivation with NAC, the maximum siROS was 0.9 mmol (g cell) $L^{-1}$, which was 4-fold lower compared to the cultivation without NAC. The corresponding $\sigma^B$ level with NAC was

**Table 3. Maximum Specific Intracellular $\sigma^B$ Transcription Levels As Indicated by $\beta$-Galactosidase, Obtained at 13 h, during Cultivation at Various Shear Levels[a]**

| shear rate, $s^{-1}$ | maximum specific intracellular transcription level of *sigB* (MU) |
|---|---|
| 0.028 | 275 ± 16 |
| 445 | 127 ± 11 |
| 1482 | 7 ± 0.5 |
| 1482 + DPI | 162 ± 12 |

[a] The NADH-oxidase (superoxide generator) inhibitor, DPI, was added at 9 h after the start of cultivation in CFB.

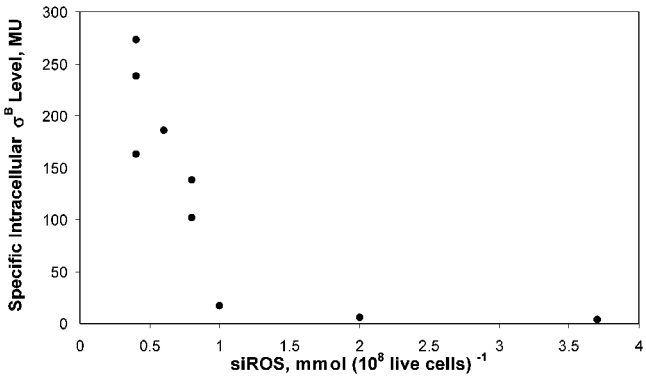


**Figure 6.** Specific intracellular $\sigma^B$ transcription levels as indicated by $\beta$-galactosidase, in Miller Units (MU), at various specific intracellular ROS level (siROS) obtained in different cultivations.

13 MU, which was about 2-fold higher compared to the cultivation without NAC. Further, when diphenylene iodoniumchloride (DPI), an inhibitor of ROS generating plasma membrane protein NADH-oxidase (NOX), was used to reduce siROS to a basal level (0.4 mmol (g cell) $L^{-1}$), the $\sigma^B$ expression increased by about 10-fold (Figure 3). These results clearly indicate that $\sigma^B$ expression under shear is regulated by intracellular levels of superoxide radical.

In addition, the siROS obtained in the $\sigma^B$ null mutants was compared with those obtained in wild-type cells under high shear (1482 $s^{-1}$) conditions. The results presented in Table 2 show that the maximum siROS in the absence of $\sigma^B$ was almost 3-fold higher compared to those obtained when $\sigma^B$ was present. This indicates that $\sigma^B$ can reduce the iROS level under high shear conditions. One of the ways in which $\sigma^B$ reduces iROS level could be by regulating the antioxidant enzymes that quench ROS, such as catalase; we had seen earlier that catalase expression is controlled by $\sigma^B$.

A possible mechanism of ROS and $\sigma^B$ involvement in determining the cell responses to shear stress is schematically shown in Figure 7.

## Conclusions

Under defined shear stress conditions, the growth, morphology, and enzyme productivity of *Bacillus subtilis* and, more importantly, its genetic responses were studied. A couette flow bioreactor with a capability to provide oxygen over the entire cultivation period without affecting the laminar flow profile was used for the study; shake flask cultivations were established as the control cultivations. Shear stress significantly affected growth characteristics, morphology, and enzyme productivity of *B. subtilis*. More interestingly, the shear level influenced gene expression. The stress transcription factor $\sigma^B$ was involved in cell responses to shear. Also, the specific

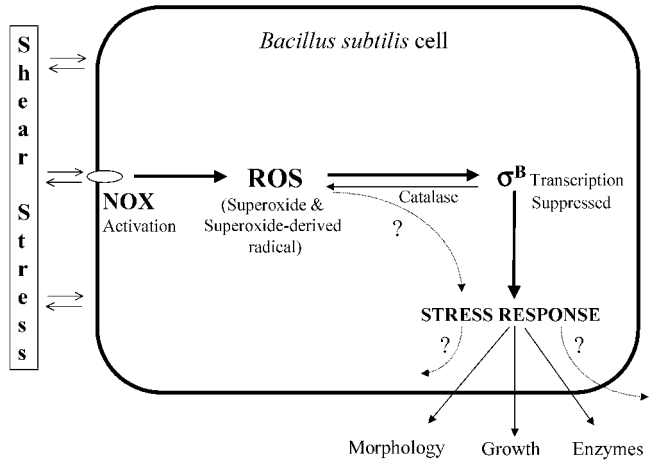


**Figure 7.** A schematic representation of some of the intracellular effects of shear stress in *Bacillus subtilis*. NOX: NADH oxidase. ROS: reactive oxygen species. $\sigma^B$: transcription factor.

intracellular reactive oxygen species level (siROS) increased with shear; the siROS and $\sigma^B$ expression under shear are interrelated.

## Acknowledgment

Department of Science and Technology, India, provided the funds. We thank Prof. W. G. Haldenwang and Prof. C. W. Price for providing the strains. We acknowledge the inputs from Rajgopal Iyer and B. Vijay Kumar, as well as the electron microscopy and ESR spectroscopy facilities provided by the Regional Sophisticated Instrumentation Center.

## Notation

$c_b$ oxygen concentration in the liquid bulk (mol $m^{-3}$)

$c_\delta$ oxygen concentration at the membrane-liquid boundary (mol $m^{-3}$)

$d_p$ particle (cell) diameter (m)

$d_s$ diameter of the rotating liquid mass (m)

$D$ diffusivity of oxygen through the membrane ($m^2$ $s^{-1}$)

$H$ Henry's law coefficient for oxygen, gas/liquid system (mol ($m^3$ N $m^{-2}$)$^{-1}$)

$H_1$ Henry's law coefficient for oxygen, gas/membrane system (mol ($m^3$N $m^{-2}$)$^{-1}$)

$H_2$ Henry's law coefficient for oxygen, membrane/liquid system (mol ($m^3$N$m^{-2}$)$^{-1}$)

$k_L$ liquid side mass transfer coefficient (m $s^{-1}$)

$k_{L,eff}$ effective liquid side mass transfer coefficient (eq 4) (m $s^{-1}$)

$n$ rotational speed ($s^{-1}$)

$N_{O_2}$ oxygen mass transfer flux (mol ($m^2$ $s^{-1}$)$^{-1}$)

$p_{O_2}$ partial pressure of oxygen in the inner cylinder (N $m^{-2}$)

$P$ power input (shake flask) (W)

$r$ any radial position in the annulus of CFB (m)

$R$ radius of the outer cylinder (m)

$Re$ Reynolds number (as defined in eq 10)

$v_\theta(r)$ tangential velocity of the fluid at the location $r$ (m $s^{-1}$)

$V_L$ liquid volume in the shake flask ($m^3$)

Greek letters

$\dot{\gamma}$ shear rate at any location in the annulus ($s^{-1}$)

$\delta$ membrane thickness (m)

$\epsilon$ rate of energy dissipation (W $kg^{-1}$)

$\eta_l$ Kolmogorov lengthscale (m)

$\kappa$ ratio of radii of the inner cylinder to the outer cylinder
$\nu$ kinematic viscosity ($m^2\ s^{-1}$)
$\Omega$ angular velocity of the outer cylinder ($s^{-1}$)
$\rho$ liquid density ($kg\ m^{-3}$)
$\tau_t$ shear stress ($N\ m^{-2}$)

## References and Notes

(1) Ma, N.; Koelling, K. W.; Chalmers, J. J. Fabrication and Use of a Transient Contractional Flow Device To Quantify the Sensitivity of Mammalian and Insect Cells to Hydrodynamic Forces. *Biotechnol. Bioeng.* **2002**, *80*, 428−437.
(2) Trinh, K.; Garcia-Briones, M.; Hink, F.; Chalmers, J. F. Quantification of Damage to Suspended Insect Cells as a Result of Bubble Rupture. *Biotechnol. Bioeng.* **1994**, *43*, 37−45.
(3) Ramirez, O. T.; Mutharasan, R. The Role of Plasma Membrane Fluidity on the Shear Sensitivity of Hybridomas Grown under Hydrodynamic Stress. *Biotechnol. Bioeng.* **1990**, *36*, 911−920.
(4) Chittur, K. K.; McIntire, L. V.; Rich, R. R. Shear Stress Effects on Human T Cell Function. *Biotechnol. Prog.* **1988**, *4*, 89−96.
(5) Mitard, A.; Riba, J. P. Morphology of *Aspergillus niger* Cultivated at Several Shear Rates. *Biotechnol. Bioeng.* **1988**, *32*, 835−840.
(6) Papadaki, M.; Eskin, S. G. Effects of Fluid Stress on Gene Regulation of Vascular Cells. *Biotechnol. Prog.* **1997**, *13*, 209−221.
(7) Arnaud, J. P.; Lacroix, C.; Foussereau, C.; Choplin, L. Shear effects on growth and activity of *Lactobacillus delbrueckii* subsp. *bulgaricus*. *J. Biotechnol.* **1993**, *29*, 157−175.
(8) Funahashi, H.; Maehara, M.; Taguchi, H.; Yoshida, T. Effects of Agitation by Flat Bladed Turbine Impeller on Microbial Production of Xanthan Gum. *J. Chem. Eng. Jpn.* **1987**, *20*, 16−22.
(9) Kieran, P. M.; O'Donnel, H. J.; Malone, D. M.; MacLoughlin, P. F. Fluid Shear Effects on Suspension Cultures of *Morinda citrifolia*. *Biotechnol. Bioeng.* **1995**, *45*, 415−425.
(10) Elias, C. B.; Desai, R. B.; Patole, M. S.; Joshi, J. B.; Mashelkar, R. A. Turbulent Shear Stress−Effect on Mammalian Cell Culture and Measurement Using Laser Doppler Anaemometer. *Chem. Eng. Sci.* **1995**, *50*, 2431−2440.
(11) Frangos, J. A.; Eskin, S. G.; Mclntire, L. V.; Ives, C. L. Flow Effects on Prostacyclin Production by Cultured Human Endothelial Cells. *Science* **1985**, *227*, 1477−1479.
(12) Edwards, N.; Beeton, S.; Bull, A. T.; Merchuk, J. C. A Novel Device for the Assessment of Shear Effects on Suspended Microbial Cultures. *Appl. Microbiol. Biotechnol.* **1989**, *30*, 190−195.
(13) Paul, E.; Mulard, D.; Blanc, P.; Fages, J.; Goma, G.; Pareilleux, A. Effects of Partial $CO_2$ Pressure and Agitation on Growth Kinetics lof *Azospirillum lipoferum* under Fermentor Conditions. *Appl. Environ. Microbiol.* **1990**, *56*, 3235−3239.
(14) Toma, M. K.; Ruklisha, M. P.; Venags, J. J.; Zeltina, M. O.; Leite, M. P.; Galinina, N. I.; Viesturs, U. E.; Tengerdy, R. P. Inhibition of Microbial Growth and Metabolism by Excess Turbulence. *Biotechnol. Bioeng.* **1991**, *38*, 552−556.
(15) ManjulaRao, Y.; Sureshkumar, G. K. Improvement in Bioreactor Productivities Using Free Radicals: HOCl-Induced Overproduction of Xanthan Gum from *Xanthomonas campestris* and Its Mechanism. *Biotechnol. Bioeng.* **2001**, *72*, 62−68.
(16) Schlichting, H. *Boundary Layer Theory*; McGraw-Hill: New York, 1955.
(17) Voelker, U.; Voelker, A.; Maul, B.; Hecker, M.; Dufour, A.; Haldenwang, W. G. Separate Mechanisms activate $\sigma^B$ of *Bacillus subtilis* in Response to Environmental and Metabolic Stresses. *J. Bacteriol.* **1995**, *177*, 3771−3780.
(18) Boylan, S. A.; Redfield, A. R.; Brody, M. S.; Price, C. W. Stress-Induced Activation of the $\sigma^B$ Transcription Factor of *Bacillus subtilis*. *J. Bacteriol.* **1993**, *175*, 7931−7937.
(19) Sarath, G.; Motte, R. S.; Wagner, F. W. Protease Assay Methods. In *Proteolytic Enzymes*: *A Practical Approach*; Beynon, R. J., Bond, J. S., Eds.; IRL Press: Oxford, 1989; pp 25−55, 25−55.
(20) Beer, R.; Sizer, F. A Spectrometric Method for the Breakdown of Hydrogen Peroxide. *J. Biol. Chem.* **1951**. *226*, 133−139.
(21) Weickert, M. J.; Chambliss, J. H. Genetic Analysis of the Promoter Region of the *Bacillus subtilis* α-Amylase Gene. *J. Bacteriol.* **1989**. *171*, 3656−3666.
(22) Nicholson, W. L.; Setlow, P. Sporulation, Germination and Out-Growth. In *Molecular Biological Methods for Bacillus*; Harwood, C. R., Cutting, S. M., Eds.; John Wiley & Sons Inc.: New York, 1990; p 442.
(23) Borg, D. C. Applications of Electron Spin Resonance in Biology. In *Free Radicals in Biology*; Pryor, W. A., Ed.; Academic Press: New York, 1976; Vol. 1, pp 69−147.
(24) Zweier, J. L. Measurement of Superoxide-Derived Free Radicals in the Reperfused Heart. *J. Biol. Chem.* **1988**. *263*, 1353−1357.
(25) Sherwood, T. K.; Pigford, R. L.; Wilke, C. R. *Mass Transfer*; McGraw-Hill: New York, 1975.
(26) Halliwell, B.; Gutteridge, J. M. C. *Free Radicals in Biology and Medicine*, 3rd ed.; Oxford University Press: Oxford, 1999.
(27) Bird, R. B.; Stewart, W. E.; Lightfoot, E. N. *Transport Phenomena*, 2nd ed.; John Wiley: New York, 2002.
(28) Henzler, H. J. Particle Stress in Bioreactors. *Adv. Biochem. Eng./Biotechnol.* **2000**. *67*, 35−82.
(29) Hsieh, H.; Cheng, C.; Wu, S.; Chiu, J.; Wung, B.; Wang, D. L. Increase of Reactive Oxygen Species (ROS) in Endothelial Cells by Shear Flow and Involvement of ROS in Shear-Induced *c-fos* Expression. *J. Cell. Physiol.* **1998**, *175*, 156−162.
(30) Yeh, L.; Park, Y. J.; Hansalia, R. J.; Imraan, I. S.; Deshpande, S. S.; Goldschmidt-Clermont, P. J.; Irani, K.; Alevriadou, B. R. Shear-Induced Tyrosine Phosphorylation in Endothelial Cells Requires Rac-1 Dependent Production of ROS. *Am. J. Physiol.* **1999**, *276*, c838-c847.
(31) Price, C. W. Protective Function and Regulation of the General Stress Response in *Bacillus subtilis* and Related Gram-Positive Bacteria. In *Bacterial Stress Responses*; Storz, G., Hengge-Aronis, R., Eds.; ASM Press: Washington, 2000; pp 179−197.
(32) Engelmann, S.; Lindner, C.; Hecker, M. Cloning, Nucleotide Sequence, and Regulation of *katE* Encoding a $\sigma^B$-Dependent Catalase in *Bacillus subtilis*. *J. Bacteriol.* **1995**. *177*, 5598−5605.

Accepted for publication July 29, 2003.

BP034191W